06

Spark Plasma Sintering of Al_2O_3-SiC ceramics. Study of the Microstructure and Properties

© M.S. Boldin,[1] A.A. Popov,[1] A.A. Murashov,[1] N.V. Sakharov,[1] S.V. Shotin,[1] A.V. Nokhrin,[1] V.N. Chuvil'deev,[1] K.E. Smetanina,[1] N.Yu. Tabachkova[2,3]

[1] Lobachevsky University of Nizhny Novgorod, Nizhny Novgorod, Russia
[2] National University of Science and Technology MISiS, Moscow, Russia
[3] Prokhorov Institute of General Physics, Russian Academy of Sciences, Moscow, Russia
e-mail: boldin@nifti.unn.ru

Received April 12, 2022
Revised July 3, 2022
Accepted July 5, 2022

The features of spark plasma sintering of submicron Al_2O_3 powders with different contents (0, 0.5, 1.5, 5 vol.%) of β-SiC nanoparticles have been studied. The microstructure and hardness of $Al_2O_3 + 5$ vol.% SiC ceramics obtained by sintering Al_2O_3 powders with β-SiC particles of various types (nanoparticles, submicron particles, fibers) have been studied. Sintering was carried out at heating rates (V_h) from 10 to 700°C/min. The sintering process of $Al_2O_3 + SiC$ ceramics with low heating rates ($V_h = 10-50$°C/min) has a complex three-stage character, with a flat area in the temperature range of 1200–1300°C. At high heating rates ($V_h > 250$°C/min), the usual three-stage character of sintering is observed. The analysis of temperature dependences of compaction was carried out using the Young-Cutler model; It was found that the kinetics of powder sintering is limited by the intensity of grain boundary diffusion. It is shown that the dependence of the hardness of $Al_2O_3 + SiC$ ceramics on V_h has a nonmonotonic character, with a maximum. In the case of pure alumina, an increase in V_h leads to a monotonic decrease in hardness

Keywords: Alumina, silicon carbide, density, diffusion, hardness.

DOI: 10.21883/TP.2022.10.54362.95-22

Introduction

Al_2O_3-SiC ceramics is widely used in industry as wear-resistant friction pairs, cutting tools, ceramic protection elements, etc. [1–3]. SiC particles make it possible to increase the mechanical properties of aluminum oxide by inhibiting the migration of grain boundaries and the formation of compressive internal stress fields that change the nature of ceramic fracture [4–9].

At present, the mechanisms of liquid-phase sintering of Al_2O_3-SiC ceramics at melting temperatures of the low-melting eutectic $Al_2O_3-SiO_2-SiC$ are well studied [10,11]. It is noted that the melting of silicon oxide present on the surface of SiC particles is accompanied by sintering acceleration, but in some cases leads to abnormal grain growth [12]. To further improve the mechanical properties of Al_2O_3-SiC ceramics, it is promising to use high-speed heating technologies that make it possible to minimize abnormal grain growth due to sintering in the solid-phase region [4,8].

Electropulse („spark") plasma sintering (ESPS) is one of the promising methods for producing ceramics with ultrafine-grained (UFG) microstructure [13]. The essence of the ESPS technology consists in high-speed (up to 2500°C/min) heating by passing high-power millisecond current pulses through a graphite mold with powder placed inside it [13]. Sintering is carried out in a vacuum or in an inert atmosphere under pressure. The advantage of the ESPS technology, which is a high-speed hot pressing method, is the ability to reduce the speed of grain boundary migration. This makes it possible to provide the improved mechanical properties of Al_2O_3-SiC [14,15] ceramics. The analysis of the publications shows that there are quite a lot of papers devoted to the ESPS of Al_2O_3-SiC ceramics [4,8,14,15], but the attention of researchers is focused on the effect of the ESPS temperature on the parameters of the microstructure and mechanical properties of ceramics. A detailed study of the heating rate effect on the parameters of the microstructure and the hardness of Al_2O_3-SiC ceramics has not been carried out.

The purpose of this paper is to study the heating rate effect on the sintering kinetics and grain growth in $Al_2O_3 + SiC$ ceramics. Pure aluminum oxide is used as the comparison object.

1. Materials and methods

The objects of study were submicron powders α-Al_2O_3 (Taimei Chemicals Co., Ltd, trade mark TM-DAR). To obtain $Al_2O_3 + SiC$ compositions, SiC powders (Alfa Aesar —

A Johnson Matthey Company) β-phases of different morphology were used: nanodispersed particles, which will be referred to below as β-SiC_n, submicron particles (β-SiC_m), and also fibers (β-SiC_w). The objects of study were compositions based on submicron powder α-Al_2O_3 (powder series № 1), with an addition of 0.5 vol.% (series № 2), 1.5 vol.% (series № 3) and 5 vol.% of β-SiC (series № 4).

The study of the effect of the type of β-SiC particles (nanoparticles, submicron particles, fibers) was carried out on the example of the composition $Al_2O_3 + 5$ vol.% β-SiC. The effect of the content of β-SiC (0, 0.5, 1.5, 5 vol.%) was studied using β-SiC_n nanopowders.

Mixing was carried out in a planetary mill FRITSCH — Pulverisette 6 in ammonia water with the addition of Dolapix CE 64 dispersant. Mixing of the powders was carried out for 24 h by grinding bodies made of ZrO_2. The grinding jar rotation frequency was 200 rev/min. Water was removed in EKPS-10 furnace (70°C, 12 h).

ESPS of samples with a diameter of 12 mm and 3 mm high was carried out using the Dr. Sinter model SPS-625 setup in graphite molds. The value of the applied uniaxial stress was $\sigma = 70$ MPa. Sintering was carried out in vacuum. Heating was carried out in a two-stage mode — heating to a temperature of 600°C at a rate of $V_h = 100$°C/min, further heating to a sintering temperature T_s at the rate of 10, 50, 100, 250, 350 or 700°C/min. The sintering temperature T_s was lower than the temperature of the beginning of abnormal grain growth in $Al_2O_3 + \beta$-SiC ceramics due to the reaction of silicon oxide present on the surface of β-SiC particles, with aluminum oxide [10–12,15]. There was no holding at the sintering temperature ($t_s = 0$ min). The samples were cooled together with the setup. To remove graphite residues, after sintering the samples were annealed in EKPS-10 air furnace at a temperature of 750°C, 1 h.

The temperature (T_1) was measured using a CHINO IR-AH2 optical pyrometer focused on the surface of the graphite mold. Based on the comparison of the readings of the pyrometer (T_1) and of the thermocouple attached to the sample surface, the values T_1 were recalculated to the sample temperature (T_2) using the empirical relation: $T_2 = \mathrm{A} \cdot T_1 - \mathrm{B}$, where A and B are constants depending on V_h.

During the ESPS the dependence of shrinkage on the heating temperature $L(T)$ was measured. The thermal expansion contribution to $L(T)$ was taken into account in accordance with the method in [16]. The shrinkage rate was calculated in a linear approximation: $S = \Delta L/\Delta t$. The $L(T)$ recalculation into the temperature dependence of compaction (ρ/ρ_{th}) was carried out in accordance with [16].

The density of ceramics (ρ) was measured by hydrostatic weighing at room temperature using a Sartorius CPA balance. The measurement accuracy ρ was ± 0.005 g/cm^3. The theoretical density (ρ_{th}) of Al_2O_3 is taken equal to 4.001 g/cm^3, and of ceramics with the addition of 0.5, 1.5 and 5% SiC — 3.997, 3.989 and 3.961 g/cm^3, respectively.

Microhardness (H_v) was measured on a hardness tester Struers Duramin-5 (load 2 kg). The value of the minimum crack resistance coefficient K_{IC} was calculated by the Palmquist method based on the length of the maximum radial crack. The measurement accuracy of H_v and K_{IC} was ± 1 GPa and ± 0.3 MPa $\cdot$ m$^{1/2}$, respectively.

The microstructure was studied using a Jeol JSM-6490 scanning electron microscope (SEM) and a Jeol JEM-2100 transmission electron microscope (TEM). The size of particles (R) and grains (d) was measured by the chord method. X-ray phase analysis (XPA) was carried out on a Shimadzu XRD-7000 diffractometer.

2. Experimental results

2.1. Certification of powders

Aluminum oxide powder has a uniform granulometric composition, the average particle size is $\sim 0.1\,\mu$m (Fig. 1, *a*). According to the XPA results, the aluminum oxide powder is single-phase, 100% α-Al_2O_3 (Fig. 2). The surface of α-Al_2O_3 nanoparticles contains an amorphous layer ~ 10 nm thick (Fig. 1, *b*).

Silicon carbide nanopowders are three-phase, X-ray patterns of β-SiC_n powder clearly show peaks of cubic phases of 98.6 wt.% 3C-SiC (PDF 00-029-1129) and 1.4 wt.% RS-SiC (PDF 00-049-1623), as well as the hexagonal phase of 6H-SiC (PDF 01-075-8314). The powders β-SiC_m and β-SiC_w are two-phase —their diffraction patterns show peaks of 6H-SiC and 3C-SiC (Fig. 2). The exact content of the phase 6H-SiC in powders β-SiC_n and β-SiC_w cannot be established — only one peak 101 of 6H-SiC is present in the diffraction patterns at diffraction angle $\sim 34°$, which merges with the more intense peak 111 of the phase 3C-SiC. The content of the phase 6H-SiC in the powder β-SiC_m is 4.1 wt.%. Peaks corresponding to silicon oxide SiO_2 (PDF 00-052-0784, 00-042-1401, 01-077-8669) were not found — probably, SiO_2 is in the X-ray amorphous state. The average size of particles β-SiC_n and β-SiC_m is ~ 50 nm and $\sim 0.8-1\,\mu$m, respectively. The length of fibers β-SiC_w reaches 50 μm, and their diameter — 200 nm.

2.2. Sintering of ceramics with different types of β-SiC particles

Fig. 3 shows the temperature dependences of $\rho/\rho_{th}(T)$ compaction for $Al_2O_3 + 5\%$ β-SiC powders with different type of silicon carbide particles. The dependences $\rho/\rho_{th}(T)$ for Al_2O_3 powders have a classical three-stage nature (see [16,17]).

As V_h increases from 10 to 700°C/min, the dependences $\rho/\rho_{th}(T)$ shift to the region of high heating temperatures. The temperature T_{90}, at which the relative density of ceramics reaches $\rho/\rho_{th}(T) = 90\%$, with V_h increasing from 10 to 700 ^{circ}C/min increases from 1220–1230 to 1380°C. The relative density of Al_2O_3 then decreases from 99.72 to 99.28% ($\rho/\rho_{th}(T) = 0.44$) (Table 1).

Dependences $\rho/\rho_h(T)$ of $Al_2O_3 + 5\%\beta$-SiC_n and $Al_2O_3 + 5\%\beta$-SiC_m ceramics have a more complex

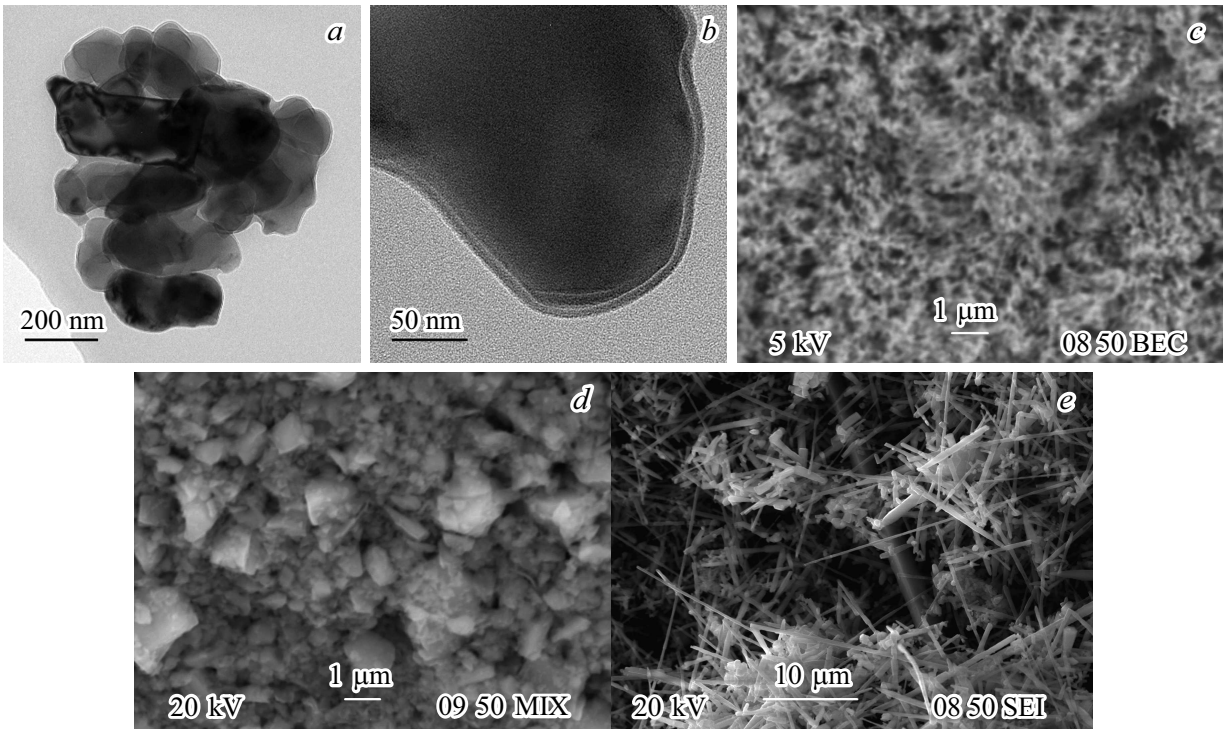

Figure 1. Electron microscope image of initial powders α-Al_2O_3 (a, b), nanoparticles β-SiC_n (c), submicron particles β-SiC_m (d) and fibers β-SiC_w (e).

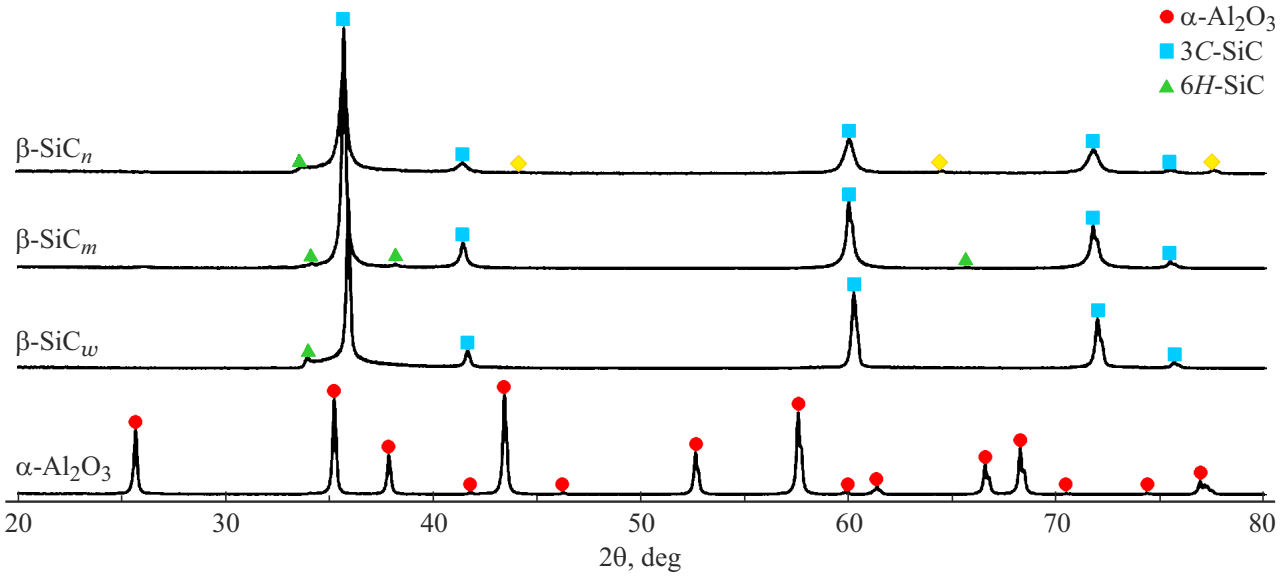

Figure 2. X-ray diffraction patterns of initial powders.

nature (Fig. 3, *b, c*) — at low heating rates (10°C/min) on the dependences $\rho/\rho_{th}(T)$, in the temperature range $\sim 1200-1300$°C a region is observed where the relative density changes little. As V_h increases, a decreasing of the temperature range is observed, corresponding to a slight change in $\rho/\rho_{th}(T) \sim 70-75\%$. At $V_h \geq 250$°C/min the dependences $\rho/\rho_{th}(T)$ have a classical three-stage nature.

The temperature T_{90} in ceramics $Al_2O_3 + 5\%\beta$-SiC_n at $V_h = 10$ and 700 ^{circ}C/min is 1410 and 1540°C, and in ceramics $Al_2O_3 + 5\%\beta$-SiC_m — 1320 and 1490°C. Thus, the addition of 5% β-SiC particles leads to a shift in the range of intense powder shrinkage to higher heating temperatures area, and the introduction of β-SiC_n nanoparticles has a more significant effect on the tem-

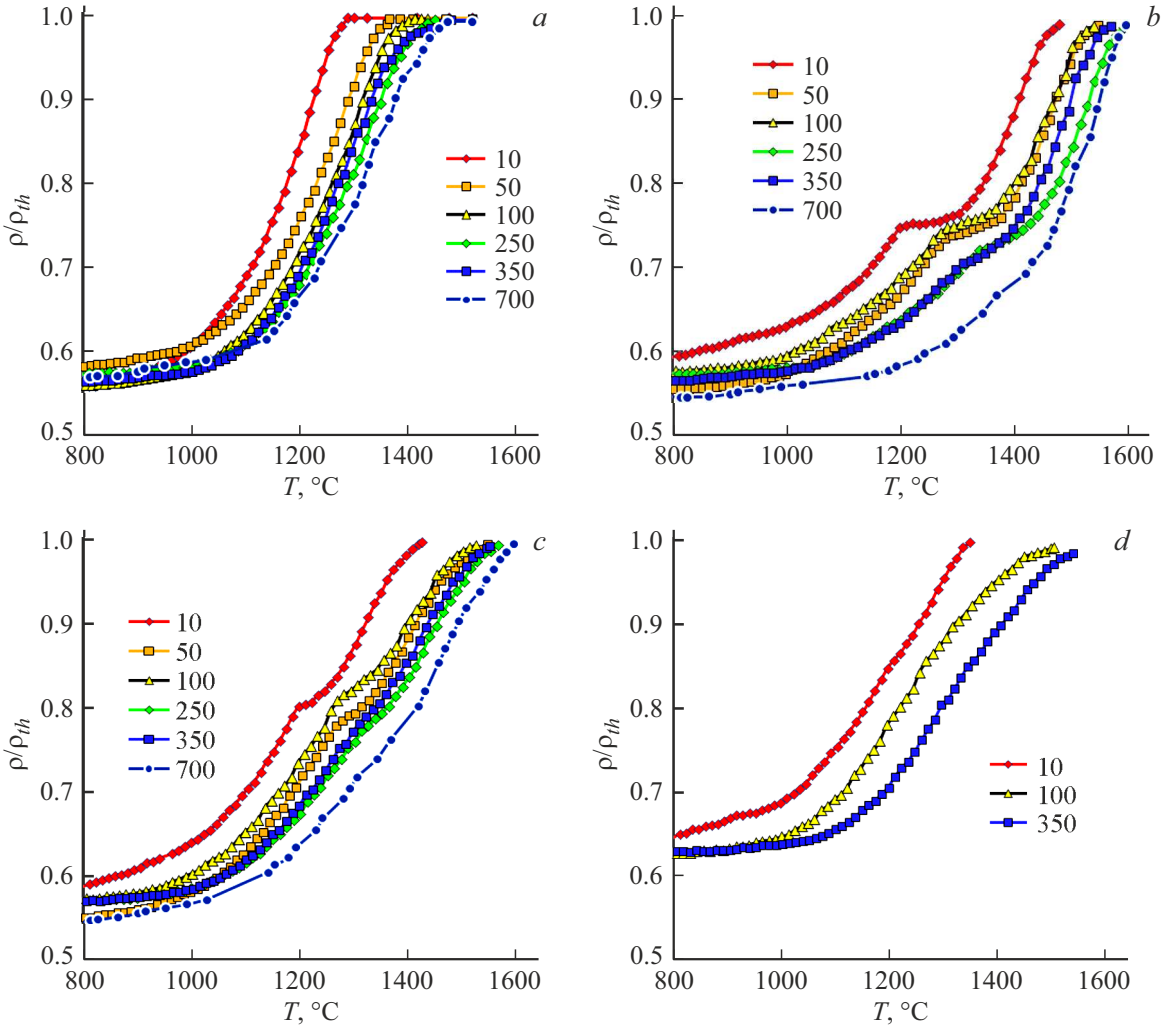

Figure 3. Compaction plots for different heating rates of powders α-Al_2O_3 (a), $Al_2O_3 + 5\%\beta$-SiC_n (b), $Al_2O_3 + 5\%$ β-SiC_m (c), $Al_2O_3 + 5\%\beta$-SiC_w (d). The heating rates are indicated on the plots.

perature T_{90} than the addition of β-SiC_m submicron particles. With V_h increasing from 10 to 700°C/min, the relative density of $Al_2O_3 + 5\%\beta$-SiC_n ceramics decreases from 99.17 to 98.96%, and of $Al_2O_3 + 5\%$ β-SiC_m ceramics — from 99.45 to 98.92%.

$\rho/\rho_{th}(T)$ sintering curves for $Al_2O_3 + 5\%$ β-SiC_w ceramics (Fig. 3, d) are similar to the compaction curves for pure Al_2O_3 (Fig. 3, a); the temperature values T_{90} at heating rates 10−350°C/min are close to the values T_{90} for Al_2O_3 at the same V_h. At V_h 10 and 350°C/min, the relative density of $Al_2O_3 + 5\%\beta$-SiC_w ceramics is 99.59 and 98.28%, respectively (Table 1). Note that at $T_s = 1520$°C, the relative density of $Al_2O_3 + 5\%\beta$-SiC ceramics is lower than the relative density of aluminum oxide in full range V_h. Emphasize also that with V_h increasing, the relative density decreasing of $Al_2O_3 + 5\%\beta$-SiC ceramics sintered at $T_s = 1520$°C is more pronounced than for pure Al_2O_3 (Table 1).

As can be seen from Table 1, the introduction of $0.5\%\beta$-SiC makes it possible to reduce the average grain size of Al_2O_3, while the amount of d decreasing with V_h increasing depends on particle shape and size. When V_h increases from 10 to 350°C/min, the value d for pure Al_2O_3 decreases from 5 to 1.8 μm (Fig. 4, a, b), and for ceramics with $5\%\beta$-SiC_n and β-SiC_w — from 0.65 to 0.4 μm and from 1.9 to 0.9 μm, respectively. The grain size of ceramics with $5\%\beta$-SiC_m does not change ($d = 0.65\,\mu$m). Thus, β-SiC_n nanoparticles have a stronger effect on the stabilization of the aluminum oxide microstructure than β-SiC_m; particles, while submicron particles have a stronger effect than fibers β-SiC_w.

Studies of the microstructure of $Al_2O_3 + 5\%\beta$-SiC_n ceramics show that β-SiC_n nanoparticles are uniformly distributed in the bulk and grain boundaries Al_2O_3 (Fig. 4, c). In most cases, several β-SiC_n particles are located together (Fig. 4, c, d), which indicates their increased tendency to agglomeration, it was not possible to overcome this by mixing the powders.

It can be seen from Fig. 4, e that in the process of mixing there was a partial fragmentation of the fibers, i.e., some

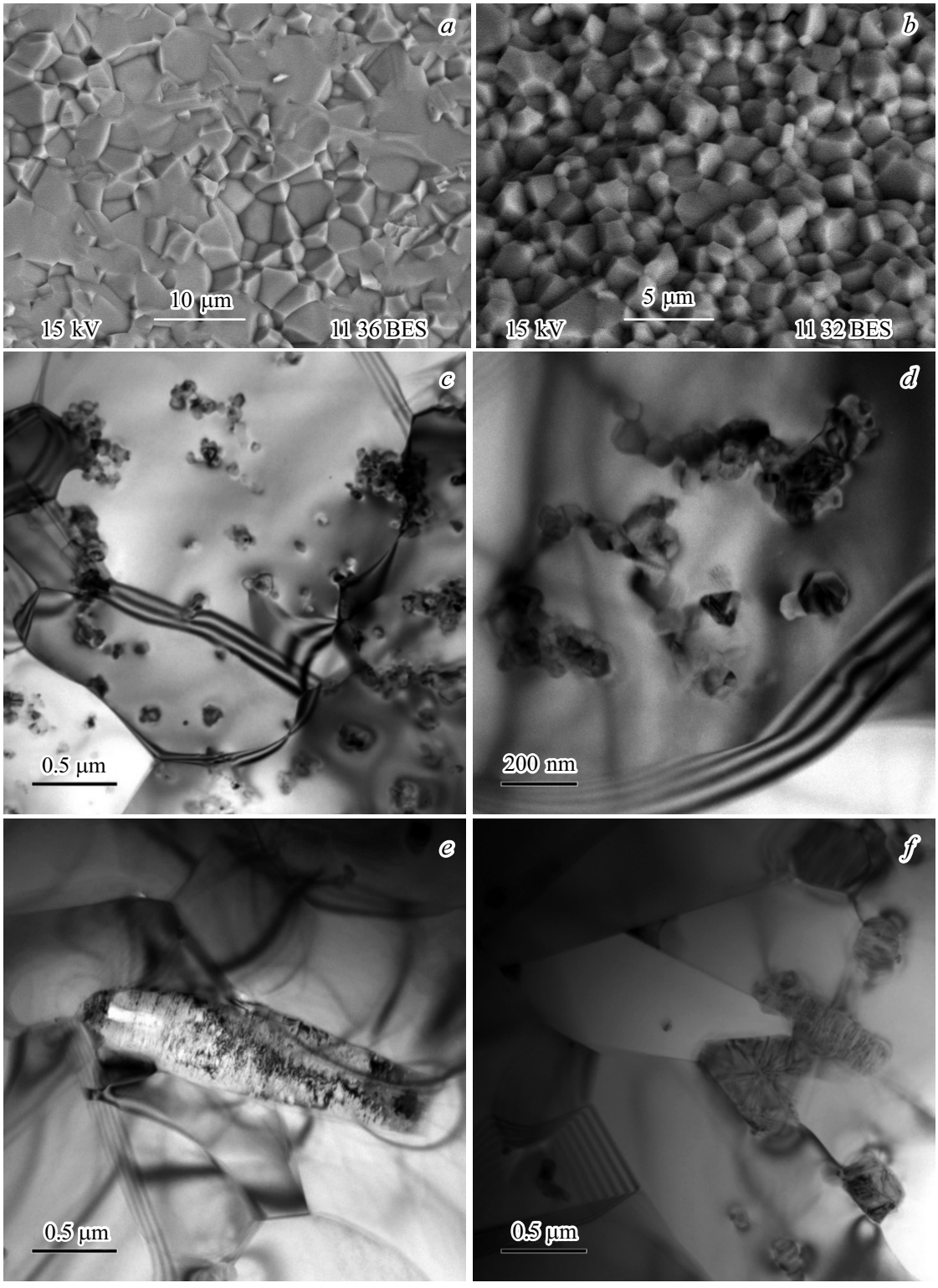

Figure 4. Microstructure of ceramics Al_2O_3 (a, b), $Al_2O_3 + 5\%\beta\text{-}SiC_n$ (c, d) and $Al_2O_3 + 5\%\beta\text{-}SiC_w$ (e, f) obtained by heating to $T_s = 1570^\circ C$ at a rate of 10 (a, c, d) and $700^\circ C$/min (b, e, f).

particles have a length of $2-3\,\mu m$. The elongated $\beta\text{-}SiC_w$ particles are located predominantly along the grain boundaries (Fig. 4, *f*). No traces of eutectic melting at the interphase boundaries of Al_2O_3 – (β-SiC) were found.

As can be seen from Table 1, the introduction of β-SiC particles and fibers increases the hardness of ceramics. Hardening with $\beta\text{-}SiC_n$ nanoparticles makes it possible to obtain ceramics with a hardness of ~ 22 GPa,

with β-SiC$_m$ particles — ceramics with a hardness of ~ 20 GPa, and with β-SiC fibers — ceramic with a hardness $H_v \sim 19$ GPa. The hardness of pure aluminium oxide lies in the range $\sim 17-19$ GPa. V_h increasing does not have a noticeable effect on the crack resistance coefficient. For all ceramics under study, the average value is $K_{IC} \sim 2.5 \pm 0.3$ MPa $\cdot$ m$^{1/2}$.

Table 1. Properties of ceramics based on aluminum oxide with addition of 5% β-SiC of various types

Ceramics	T_s, °C	V_h, °C/min	d, μm	ρ/ρ_{th}, %	H_v, GPa	K_{IC}, MPa $\cdot$ m$^{1/2}$
Al_2O_3	1520	10	5.1	99.72	18.6	2.5
		50	3	99.67	18.2	2.3
		100	2.8	99.60	17.9	2.5
		250	2	99.47	17.8	2.4
		350	1.9	99.47	17.2	2.1
		700	1.8	99.28	16.9	2.4
$Al_2O_3 + 5\%\,SiC_n$	1520	10	0.45	98.53	21.4	2.5
		100	0.2	96.50	21.4	2.6
		350	0.2	94.81	19.9	2.6
	1570	10	0.65	99.17	20.1	3.0
		50	0.4	99.09	21.5	2.5
		100	0.4	99.03	–	–
		250	0.4	98.88	22.0	2.6
		350	0.4	98.96	22.1	2.5
		700	0.4	98.96	21.8	2.0
$Al_2O_3 + 5\%\,SiC_m$	1520	10	0.6	99.05	20.5	2.8
		100	0.55	97.83	20.3	2.7
		350	0.45	97.54	20.2	2.7
	1570	10	0.65	99.45	19.6	2.6
		50	0.65	99.18	20.3	2.5
		100	0.65	99.08	20.5	2.2
		250	0.65	99.14	20.4	2.1
		350	0.65	99.05	20.0	2.1
		700	0.65	98.92	19.8	2.1
$Al_2O_3 + 5\%\,SiC_w$	1520	10	0.9	99.04	19.4	2.3
		100	0.7	98.08	19.5	2.2
		350	0.6	97.12	17.8	2.2
	1570	10	1.9	99.59	19.0	2.6
		100	0.9	99.00	18.9	2.2
		350	0.9	98.28	18.9	2.2

Table 2. Microstructure parameters and mechanical properties of ceramics with different contents of β-SiC$_n$ nanoparticles

β-SiC$_n$. %	T_s, °C	V_h, °C/min	d, μm	ρ/ρ_{th}, %	H_v, GPa	K_{IC}, MPa $\cdot$ m$^{1/2}$
0.5	1520	10	0.99	99.66	19.7	2.7
		50	0.89	99.37	20.8	2.4
		100	0.84	99.29	20.6	2.4
		250	0.70	99.05	20.8	2.3
		350	0.67	98.78	21	2.4
		700	0.62	98.61	20.6	2.4
1.5	1520	10	0.72	99.71	20	3.0
		50	0.62	99.35	20.9	2.6
		100	0.57	98.73	21	2.6
		250	0.45	98.40	21	2.4
		350	0.45	98.40	21.3	2.3
		700	0.26	98.21	21.1	2.2

It is important to note the nature of the V_h effect on H_v ceramics. As can be seen from Table 1, V_h increasing from 10 to 700°C/min leads to H_v of aluminum oxide decreasing from 18.6 to 16.9 GPa. The dependence $H_v(V_h)$ for $Al_2O_3 + 5\%\beta$-SiC ceramics is nonmonotonic, with a maximum. The heating rate, at which the maximum value H_v is reached, depends on the sintering temperature and the type of β-SiC particles (Table 1).

2.3. Sintering of ceramics with different content of β-SiC

Figs. 3, *b* and 5 show the dependences $\rho/\rho_{th}(T)$ for Al_2O_3 powders with different contents of nanoparticles β-SiC$_n$. It can be seen from a comparison of the Figures that at $V_h = 10$°C/min the increasing of the bulk fraction of β-SiC$_n$ particles leads to the increasing of the temperature range, in which the nonmonotonic nature of the dependence $\rho/\rho_{th}(T)$ is observed, to the decreasing of the relative density of ceramics, at which a plateau of the $\rho/\rho_{th}(T)$ curve is observed. Note also that β-SiC$_n$ content increasing from 1.5 to 5 vol.% leads to the temperature T_{90} increasing from 1250 to 1410°C at $V_h = 10$°C/min and from 1450 to 1540°C at $V_h = 700$°C/min (Fig. 3, *b*, 5, *a*). The relative density of ceramics sintered at $T_s = 1520$°C decreases from 98.78 to 98.53% at $V_h = 10$°C/min and from 98.61 to 94.81% at $V_h = 700$°C/min (Table 1, 2). Thus, β-SiC$_n$ particles content increasing leads to the dependences $\rho/\rho_{th}(T)$ shift to higher temperatures and the relative density of ceramics decreasing.

As can be seen from Table 2, the addition of 0.5% β-SiC makes it possible to reduce the average ceramic grain size ($T_s = 1520$°C) by more than 2 times and

form an UFG microstructure in aluminum oxide. In $Al_2O_3 + 5$ vol.% β-SiC_n, ceramics sintered at heating rates of 10 and 700°C/min ($T_s = 1570$°C), the average grain size is 0.65 and 0.4 μm, respectively. Thus, in accordance with the Zener equation [9], the increased volume fraction of β-SiC_n nanoparticles leads to the average size decreasing of ceramic grain.

As can be seen from Tables 1 and 2, the introduction of β-SiC_n leads to the increased microhardness of ceramics over the entire range of heating rates under study, while the crack resistance coefficient changes insignificantly. Addition of 0.5%vol. β-SiC_n increases H_v of ceramics from 17 to ~ 21 GPa. A similar value of hardness is observed in $Al_2O_3 + 1.5\%\beta$-SiC_n ceramics (Table 2). In our opinion the hardness decreasing of $Al_2O_3 + 5\%\beta$-SiC_n ceramics is due to the decreasing of its relative density (Table 1). The crack resistance coefficient of the studied ceramics varies insignificantly and lies in the range $2.5-3\,\mathrm{MPa}\cdot\mathrm{m}^{1/2}$.

3. Summary and analysis of results

To analyze the ESPS kinetics of $Al_2O_3 + \beta$-SiC powders, we use the Yang

-

Cutler model [18], which describes the process of non-isothermal sintering of spherical particles under conditions of the simultaneous flow of processes of bulk and grain boundary diffusion, as well as plastic deformation (creep). In accordance with [18], the slope of the temperature dependence of the relative shrinkage (ε) in the coordinates $\ln(T\partial\varepsilon/\partial T) - T_m/T$ corresponds to the effective sintering activation energy mQ_s, where $T_m = 2326$ K is Al_2O_3 melting point, m is coefficient depending on the dominant sintering mechanism ($m = 1/3$ — for the case of grain boundary diffusion, $m = 1/2$ — for bulk diffusion, $m = 1$ for viscous material flow (creep)). In the case of ESPS of submicron powders the value of the coefficient m can be taken equal to 1/3 [19].

The value of the effective activation energy mQ_s during ESPS of submicron powders Al_2O_3 lies in the range of ~ 5.6 to $6.2\,\mathrm{kT}_m$ and practically does not depend on the heating rate V_h (Fig. 6, *a*). At $m = 1/3$, the activation energy of ESPS of Al_2O_3 powders is $\sim 16.8-18.0\,\mathrm{kT}_m$ ($\sim 325-360$ kJ/mol). The value obtained is close to the activation energy of grain boundary diffusion of oxygen in aluminum oxide ($Q_b \sim 380$ kJ/mol $\sim 19.7\,\mathrm{kT}_m$ [20]). The dependences $\ln(T\partial\varepsilon/\partial T) - T_m/T$ for ceramics $Al_2O_3 + 5\%$ β-SiC_w,, whose slope angle corresponds to the effective activation energy $mQ_s \sim 4.6-5.8\,\mathrm{kT}_m$, have the similar nature. Thus, we can conclude that the sintering kinetics of fine-grained powders of pure Al_2O_3 and $Al_2O_3 + 5$ vol.% β-SiC is limited by the intensity of grain boundary diffusion.

Note that in the case of β-SiC nanopowders, which have a large free surface area, the plateau of the dependence $\rho/\rho_{th}(T)$ in the temperature range $\sim 1200-1300$°C is the most evident (Fig. 6, *b*). The free surface area decreasing (the size of β-SiC particles increasing) leads to a decreased length of the plateau in the dependence $\rho/\rho_{th}(T)$ (Fig. 6, *c*). In the case of β-SiC_w fibers this section is almost invisible on the dependence $\rho/\rho_{th}(T)$ (Fig. 6, *d*). Since the volume fraction of β-SiC_n, β-SiC_m and β-SiC_w particles is the same (5 vol.%), one can suggest that the phase composition of the silicon carbide powder, as well as the concentration of oxygen atoms adsorbed on the surface of β-SiC particles have a significant effect on the intensity of the polymorphic transformation process. Summarizing the XPA results shows that in the nanopowder β-SiC_n contains a cubic phase RS-SiC (PDF 00-049-1623), which is absent in powders β-SiC_m and β-SiC_w.

For $Al_2O_3 + \beta$-SiC_n and $Al_2O_3 + \beta$-SiC_m ceramics, the dependence $\ln(T\partial\varepsilon/\partial T) - T_m/T$ can be interpolated by two straight lines with different slopes (Fig. 6, *b*). Note that the effective activation energy of the ESPS in the low-temperature region is close to the activation energy of the ESPS of pure aluminum oxide (Fig. 6, *a*), and at higher heating temperatures it reaches $mQ_s \sim 11-13\,\mathrm{kT}_m$. At present, the exact reasons for the activation energy increasing of ESPS of aluminum oxide powders with the addition of SiC nanoparticles were not determined.

In our opinion, one of the reasons may be the presence of the increased concentration of adsorbed oxygen and/or silicon oxide on the surface of β-SiC_n nanoparticles. The oxygen presence on the surface of carbide nanoparticles can have a significant effect on the ESPS [17,21] kinetics and mechanical properties [21,22] of fine-grain ceramics. It was noted in paper [11] that at temperatures below 1600°C the β-SiC phase can react with the SiO_2 surface layer to form SiO and CO. The formation of gaseous reaction products can hinder the sintering of aluminum oxide powders and be one of the reasons for the increasing of the ESPS activation energy. Note that the heating rate increasing should lead to the reaction intensity decreasing in the $Al_2O_3-SiO_2-SiC$ system and, as a consequence, to the disappearance of the plateau on the dependence $\rho/\rho_{th}(T)$, which is in good agreement with the experimental data (Fig. 3, *b, c*).

Let us analyze the features of grain growth in fine-grained $Al_2O_3 + \beta$-SiC ceramics. It can be seen from Tables 1 and 2, that β-SiC particles prevent the growth of aluminum oxide grains and make it possible to form UFG microstructure in the ceramics. The analysis of the results of microstructure studies presented in Table 1 shows that the dependence $d(R)$ can be described with good accuracy by straight lines (Fig. 7). The highest values of the confidence factor of the linear approximation (R^2) are achieved in the case of heating at low rates (10°C/min). Under conditions of high-speed heating, which leads to the decreasing of the relative density of ceramics (Table 1, 2), the coefficient R^2 decreases. In our opinion, this is due to the presence of pores, which also prevent the migration of grain boundaries [17].

Using the data presented in Tables 1 and 2, we analyzed the effect of the volume fraction of β-SiC nanoparticles (0, 0.5, 1.5, 5 vol.%) on the average grain size (d) of

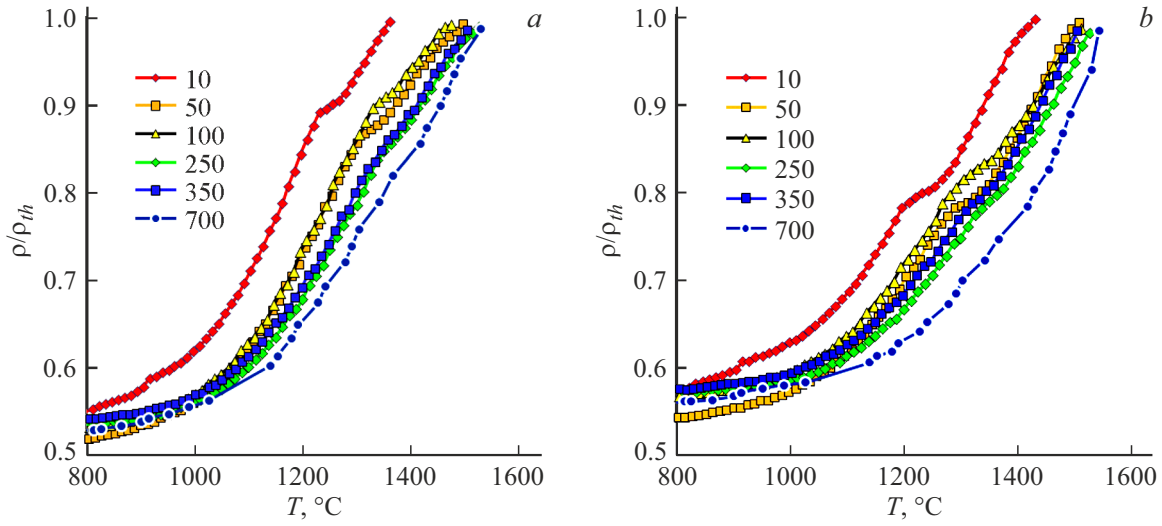

Figure 5. Compaction curves for Al_2O_3 powders with 0.5 (a) and 1.5% β-SiC_n (b) for different V_h.

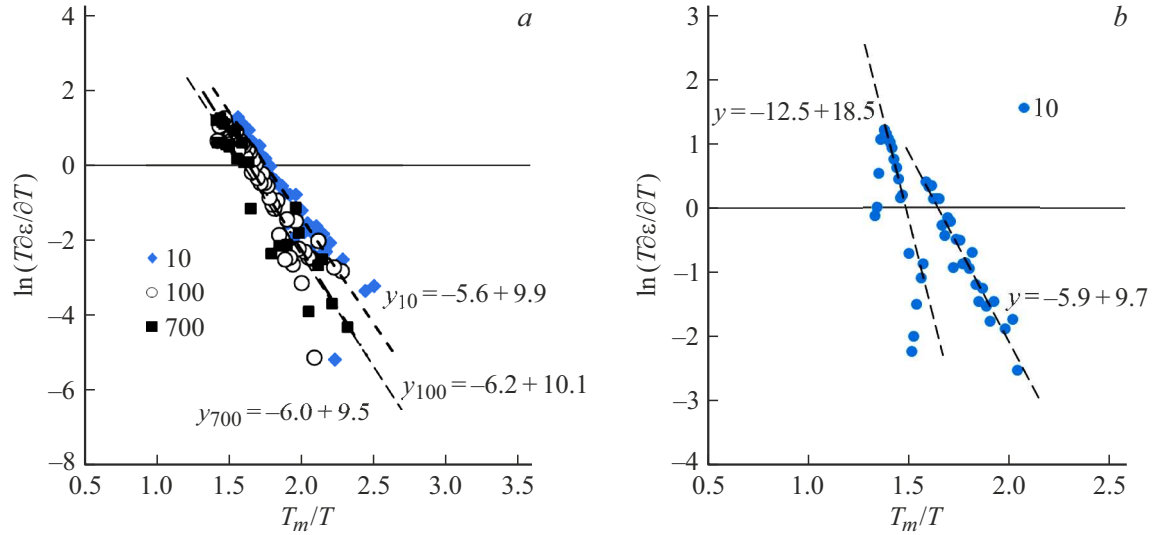

Figure 6. Temperature dependences of shrinkage in coordinates $\ln(T\partial\varepsilon/\partial T)-T_m/T$: Al_2O_3 (a); $Al_2O_3 + 5\%\beta$-SiC_n (b). The heating rates are indicated on the graphs.

aluminum oxide. The highest values of the coefficient $R^2 = 0.97-0.99$ were achieved in the case of linear interpolation of the dependence $d(f_v)$ in the coordinates $d-f_v^{-1/3}$ (Fig. 7, b). This indicates that the Hillert–Hellman relation ($d/R = 3.6f_v^{-1/3}$) [23] more correctly describes the obtained experimental results compared to the usual Zener relation $d/R = 4/(3f_v)$ [9,23]. The average value of the coefficient R^2 in the coordinates of the dependence $d(f_v)$ in the coordinates $d-1/f_v$ is $R^2 = 0.94$.

Let us now analyze the effect of the grain size and β-SiC particles on the hardness of ceramics. Note preliminarily that the porosity and state of grain boundaries also have a significant effect on the mechanical properties of ceramics. This is most clearly seen in the example of pure aluminium oxide. As can be seen from Table 1, the heating rate increasing from 10 to 700°C/min leads to the relative density decreasing from 99.72 to 99.28% and, as a consequence, to the hardness decreasing from 18.6 to 16.9 GPa. Thus, a relatively small relative density decreasing ($\rho/\rho_{th} = 0.44\%$) leads to the hardness decreasing of aluminum oxide by 1.7 GPa. The result obtained is rather unexpected, since with V_h increasing, simultaneously with the relative density decreasing of ρ/ρ_{th}, d decreasing from 5.1 to 1.8 μm is observed. Nevertheless, the factor of relative density decreasing turns out to be more significant for the hardness of aluminum oxide than d decreasing by ~ 2.8 times.

In our opinion, a special non-equilibrium state of grain boundaries has an indirect effect on the hardness decreasing of aluminum oxide with a small grain size. As can be seen from Fig. 1, b, there is an amorphous layer on the surface of submicron particles Al_2O_3, which crystallizes during ESPS

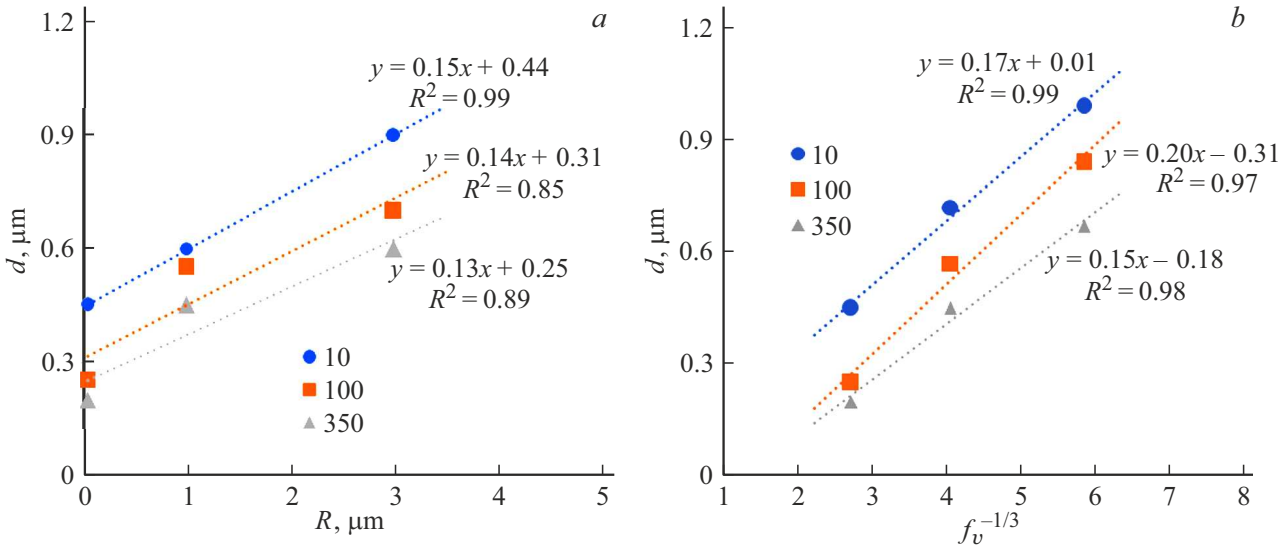

Figure 7. Dependence of average grain size (d) of aluminum oxide on the size (R) (a) and volume fraction (f_v) of β-SiC particles (b). $T_s = 1520^\circ$C. The heating rates (10, 100, 350°C/min) are shown in the Figures.

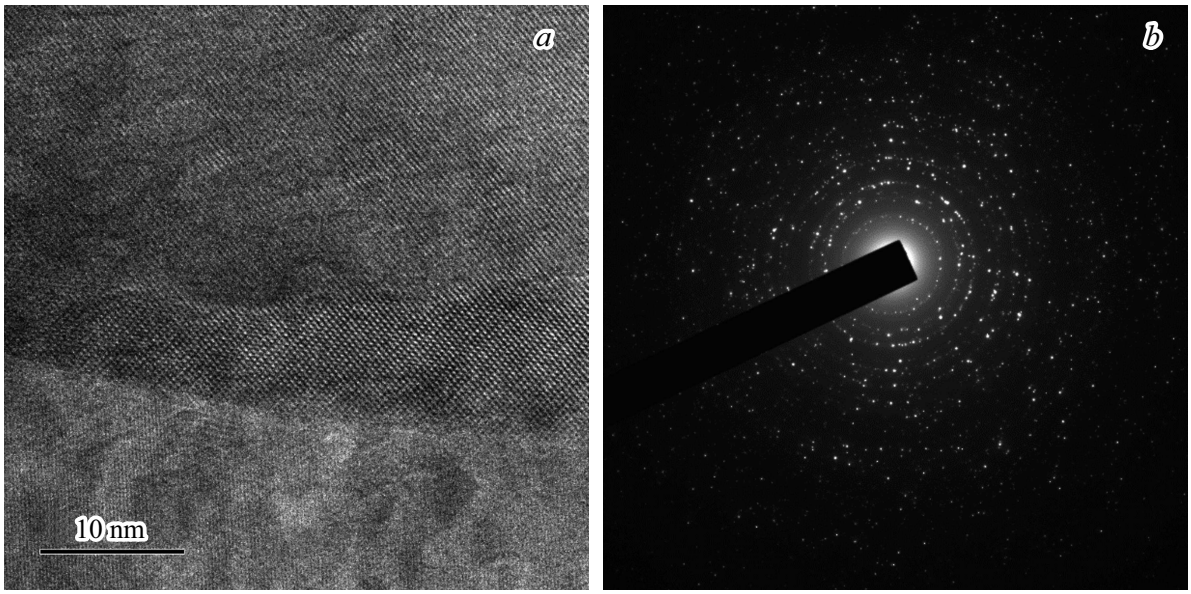

Figure 8. Electron-microscopic image of grain boundary in Al_2O_3 (a) ceramics and annular electron diffraction pattern (b) corresponding to this section of the microstructure. ESPS modes: $V_h = 350^\circ$C/min, $T_s = 1520^\circ$C, $t_s = 0$ min.

and transforms into ceramic grain boundaries (Fig. 8). The results of electron microscopic studies did not reveal the presence of the amorphous phase at the grain boundaries of aluminum oxide.

The amorphous phase contains an excess free volume [24], and during its crystallization the defects of the vacancy and dislocation type [25] can appear. This can lead to the volume fraction increasing of non-equilibrium grain boundaries containing excess free volume [25,26]. High-speed heating leads to the total duration decreasing of the sintering process and, as a result, reduces the degree of relaxation of the non-equilibrium structure of grain boundaries. The presence of defects at the grain boundaries can have a significant effect on the hardness of aluminium oxide, and is one of the factors affecting the relative density decreasing of samples obtained at high heating rates.

A simultaneous decreasing of the relative density and grain size with the heating rate increasing makes it possible to explain the nonmonotonic, with a maximum, nature of the dependence $H_v(V_h)$ for $Al_2O_3 + \beta$-SiC ceramics (Fig. 9). The addition of β-SiC_n nanoparticles makes it possible to decrease the grain size and to increase the hardness of aluminum oxide. As V_h increases, the average grain size

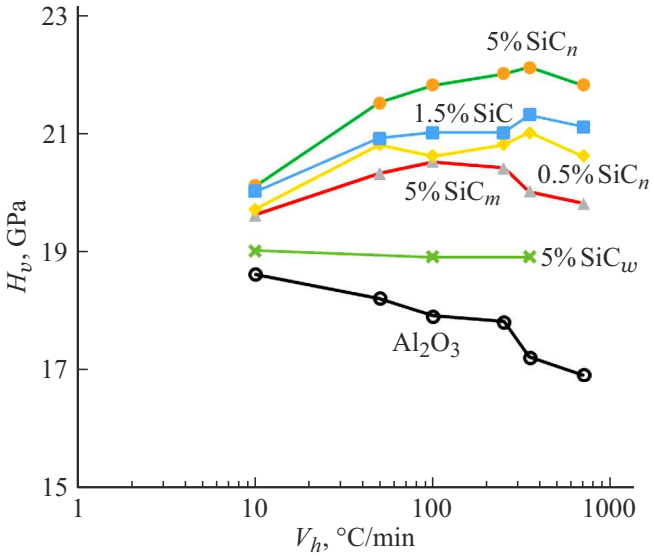

Figure 9. Hardness of aluminum oxide and $Al_2O_3 + \beta$-SiC ceramics vs. heating rate.

decreasing leads to H_v increasing. The hardness decreasing at large V_h is due to the simultaneous decreasing of the relative density of ceramics and the increased density of defects at the grain boundary of aluminum oxide.

Thus, from a practical point of view, to ensure high hardness characteristics of aluminum oxide it is necessary to use intermediate ESPS heating rates ($V_h = 100-350$°C/min), at which the grain size reduction factor will dominate over the negative influence of the reduced relative density of ceramics.

Conclusion

1. The nature of the temperature dependence of $\rho/\rho_{th}(T)$ compaction of $Al_2O_3 + \beta$-SiC powders is determined by the heating rate V_h and the dispersion of the β-SiC particles. At low heating rates (10–50°C/min) of aluminum oxide powders with the addition of β-SiC nano- and microparticles, the dependences $\rho/\rho_{th}(T)$ have nonmonotonic character with a plateau in the temperature range 1200–1300°C. At high heating rates ($V_h > 250$°C/min) the dependences $\rho/\rho_{th}(T)$ have the usual three-stage nature.

2. The heating rate increasing leads to the average grain size decreasing of aluminum oxide and $Al_2O_3 + \beta$-SiC ceramics. The dependence of the average grain size (d) on the volume fraction (f_v) and size (R) of silicon carbide particles is described with good accuracy by the Hillert–Hellman equation: $d/R = 3.6 f_v^{-1/3}$.

3. Hardness vs. heating rate of $Al_2O_3 + \beta$-SiC ceramics has a nonmonotonic nature, with a maximum. The maximum hardness values of $Al_2O_3 + \beta$-SiC ceramics are reached at $V_h = 100-350$°C/min. The nonmonotonicity of the dependence $H_v(V_h)$ is due to the average grain size decreasing, the relative density decreasing of ceramics, and the formation of non-equilibrium state of grain boundaries with the heating rate V_h increasing.

Funding

This study was supported financially by the Russian Science Foundation (grant No 20-73-10113). The study by transmission electron microscopy was performed on the equipment of the Center for Collective Use Materials Science and Metallurgy NUST MISIS (project of the Russian Ministry of Education and Science № 075-15-2021-696).

Conflict of interest

The authors declare that they have no conflict of interest.

References

[1] Z. Yin, S. Yan, J. Ye, Z. Zhu, J. Yuan. Ceramics Int., **45** (13), 16113 (2019). DOI: 10.1016/j.ceramint.2019.05.128
[2] E. Gevorkyan, A. Mamalis, R. Vovk, Z. Semiatkowkski, D. Morozow, V. Nerubatskyi, O. Morozova. JINST, **16**, P10015 (2021). DOI: 10.1088/1748-0221/16/10/P10015
[3] M.S. Boldin, N.N. Berendeev, N.V. Melekhin, A.A. Popov, A.V. Nokhrin, V.N. Chuvil'deev. Ceramics Int., **47** (18), 25201 (2021). DOI: 10.1016/j.ceramint.2021.06.066
[4] J.H. Chae, K.H. Kim, Y.H. Choa, J. Matsushita, J.-W. Yoon, K.B. Shim. J. Alloys Compd., **413** (1–2), 259 (2006). DOI: 10.1016/j.jallcom.2005.05.049
[5] I. Monohjimoh, M.A. Hussein, N. Al-Aqeeli. Nanomaterials, **9** (1), 86 (2019). DOI: 10.3390/nano9010086
[6] X.L. Shi, F.M. Xu, Z.J. Zhang, Y.L. Dong, Y. Tan, L. Wang, J.M. Yang. Mater. Sci. Eng. A., **527** (18–19), 4646 (2010). DOI: 10.1016/j.msea.2010.03.035
[7] Y.L. Dong, F.M. Xu, X.L. Shi, C. Zhang, Z.J. Zhang, J.M. Yang, Y. Tan. Mater. Sci. Eng. A, **504** (1–2), 49 (2009). DOI: 10.1016/j.msea.2008.10.021
[8] J. Liu, Z. Li, H. Yan, K. Jiang. Adv. Eng. Mater., **16** (9), 1111 (2014). DOI: 10.1002/adem.201300536
[9] Y. Xu, A. Zangvil, A. Kerber. J. Eur. Cer. Soc., **17** (7), 921 (1997). DOI: 10.1016/S0955-2219(96)00164-1
[10] S. Gustafsson, L.K.L. Falk, E. Lidén, E. Carlström. Ceramics Int., **34** (7), 1609 (2008). DOI: 10.1016/j.ceramint.2007.05.005
[11] D. Galusek, R. Klement, J. Sedláček, M. Balog, C. Fasel, J. Zhang, M.A. Crimp, R. Riedel. J. Eur. Cer. Soc., **31** (1–2), 111 (2011). DOI: 10.1016/j.jeurceramsoc.2010.09.013
[12] C.C. Anya, S.G. Roberts. J. Eur. Cer. Soc., **17** (4), 565 (1997). DOI: 10.1016/S0955-2219(96)00092-1
[13] M. Tokita. Ceramics, **4** (2), 160 (2021). DOI: 10.3390/ceramics4020014
[14] L. Gao, H.Z. Wang, J.S. Hong, H. Miyamoto, K. Miyamoto, Y. Nishikawa, S.D.D.L. Torre. J. Eur. Cer. Soc., **19** (5), 609 (1999). DOI: 10.1016/S0955-2219(98)00232-5
[15] I. Álvarez, R. Torrecillas, W. Solis, P. Peretyagin, A. Fernández. Ceramics Int., **42** (15), 17248 (2016). DOI: 10.1016/j.ceramint.2016.08.019

[16] V.N. Chuvil'deev, M.S. Boldin, Ya.G. Dyatlova, V.I. Rumyantsev, S.S. Ordan'yan. Rus. J. Inorg. Chem., **60** (8), 987 (2015). DOI: 10.1134/S0036023615080057
[17] M.N. Rahaman. *Ceramic Processing and Sintering* (Marcel Dekker Inc., NY., 2003)
[18] W.S. Young, I.B. Culter. J. Am. Ceramic Soc., **53** (12), 659 (1970). DOI: 10.1111/j.1151-2916.1970.tb12036.x
[19] M.S. Boldin, A.A. Popov, E.A. Lantsev, A.V. Nokhrin, V.N. Chuvil'deev. Materials, **15** (6), 2167 (2022). DOI: 10.3390/ma15062167
[20] H.J. Frost, M.F. Ashby. *Deformation Mechanism Maps: The Plasticity and Creep of Metals and Ceramics* (Pergamon Press, Oxford, 1982)
[21] E.A. Lantsev, N.V. Malekhonova, Y.V. Tsvetkov, Y.V. Blagoveshchensky, V.N. Chuvil'deev, A.V. Nokhrin, M.S. Boldin, P.V. Andreev, K.E. Smetanina, N.V. Isaeva. Inorganic Mater.: Appl. Res., **12** (3), 650 (2021). DOI: 10.1134/S2075113321030242
[22] A. Bokov, A. Shelyug, A. Kurlov. J. Eur. Cer. Soc., **41** (12), 5801 (2021). DOI: 10.1016/j.jeurceramsoc.2021.05.007
[23] D. Fan, L.-Q. Chen, S.-P.P. Chen. J. Am. Ceramic Soc., **81** (3) 526 (1998). DOI: 10.1111/j.1151-2916.1998.tb02370.x
[24] V.I. Betekhtin, A.G. Kadomtsev, A.Yu. Kipyatkova, A.M. Glezer. Phys. Solid State, **40** (1), 74 (1998). DOI: 10.1134/1.1130237
[25] V.N. Chuvildeev. *Neravnovesnye granitsy zeren v metallakh. Teoriya i prilozheniya* (Fizmatlit, M., 2004) (in Russian)
[26] A.B. Mazitov, A.R. Oganov. Zapiski Rossiiskogo Mineralogicheskogo Obshchestva (Proceedings of the Russian Mineralogical Society), **150** (5), 92 (2021). DOI: 10.31857/S086960552105004X